

Feasibility Study of Wood-Leaf Separation Based on Hyperspectral LiDAR Technology in Indoor Circumstances

Hui Shao , Zheng Cao , Wei Li , Yuwei Chen , Changhui Jiang , Juha Hyypä, Jie Chen, and Long Sun

Abstract—Wood-leaf separation aiming at classifying LiDAR points into wood and leaf components is one of the most important genres for improving leaf area index estimation and forestry survey accuracy. The wood return signals could artificially increase the apparent foliage content, which needs to be screened out for deriving vital tree attributes accurately. Previous research works tended to use intensity, waveform, and geometric information extracted from a single wavelength LiDAR for wood-leaf separation. This article employs a revised hyperspectral LiDAR (HSL) to obtain spatial and ultrawide spectral data simultaneously. We also propose a simple three steps method to separate wood and leaf components based on HSL spatial and spectral measurements under the laboratory circumstances. First, the preprocessing is conducted to acquire 3-D spatial information and the multiband laser pulse reflectance for further separation. Second, preliminary separation (band division, key feature parameter calculation, and judgment) is implemented based on reflectance. Third, we employ K-Nearest Neighbor (KNN) method to enhance separation results based on preliminary separation results and spatial features and then update the results by recorrection. Then, 3-D reconstruction is accomplished by fusing wood-leaf separation results. The experimental results demonstrate that the proposed method can separate wood and leaf components with high accuracy and indicate tree attributes straightforwardly.

Index Terms—Hyperspectral LiDAR (HSL), reflectance, spatial coordinate, wood-leaf separation.

Manuscript received August 4, 2021; revised October 7, 2021 and November 16, 2021; accepted December 4, 2021. Date of publication December 13, 2021; date of current version January 10, 2022. This work was supported in part by the University Synergy Innovation Program of Anhui Province under Grant GXXT-2019-007, in part by the Anhui Provincial Natural Science Foundation under Grant 2008085MF182 and Grant 1708085MD90, in part by the Research Program of Anhui Jianzhu University under Grant JZ202022, in part by the Academy of Finland projects Ultrafast Data Production with Broadband Photodetectors for Active Hyperspectral Space Imaging under Grant 336145, in part by the Forest-Human-Machine Interplay - Building Resilience, Redefining Value Networks and Enabling Meaningful Experiences (UNITE) under Grant 337656, in part by the Strategic Research Council project Competence-Based Growth Through Integrated Disruptive Technologies of 3D Digitalization, Robotics, Geospatial Information and Image Processing/Computing - Point Cloud Ecosystem under Grant 314312, and in part by the Jihua lab under Grant X190211TE190 and Huawei under Grant 9424877. (Corresponding author: Hui Shao.)

Hui Shao, Zheng Cao, Jie Chen, and Long Sun are with the School of Electronic and Information Engineering, Anhui Jianzhu University, Hefei 230601, China (e-mail: shaohui@ahjzu.edu.cn; 2455373203@qq.com; chenjie@ahjzu.edu.cn; sunlong126@126.com).

Wei Li is with the Institute of Unmanned System, Beihang University, Beijing 100191, China (e-mail: liwei_buaa@buaa.edu.cn).

Yuwei Chen, Changhui Jiang, and Juha Hyypä are with the Finnish Geospatial Research Institute, FI-02430 Masala, Finland (e-mail: yuwei.chen@nls.fi; changhui.jiang1992@gmail.com; juha.hyypa@nls.fi).

Digital Object Identifier 10.1109/JSTARS.2021.3134651

I. INTRODUCTION

DESCRIBING forest 3-D structure is of broad importance, which helps to investigate species competition, wood production, and ecosystem dynamics. New developments in LiDAR provide unprecedented detail and geometric accuracy information of trees and forests, allowing improved estimates of high-resolution 3-D measurements of tree and forest structures. LiDAR can generally be categorized into three types based on their platform: satellite-based, airborne-based, and ground-based LiDAR [1], [2]. The ground-based LiDAR has attracted increasing attention for providing an accurate and flexible way of quantifying tree characteristics underneath the forest canopy, compensating for details of other technologies rendering data [3], [4]. Coupled with retrievals of the above-ground woody biomass information, terrestrial LiDAR, as one commonly used ground-based LiDAR, provides a methodology that should measure forest structure more rapidly and with less field effort than standard forestry methods [5].

Leaf area index (LAI), foliage profile, and stand height are critical vegetation structural parameters for bio-geoscience applications [6]. Especially, LAI is a biophysical parameter of vegetation applied in many applications, typically derived by regressions between ground-truth vegetation index and spectral or angular information from airborne or satellite imagery [7], [8]. For the structural complexity and spatially variability, it is difficult to measure and describe forest structure accurately. Nonphotosynthetic components of forest canopies, including branches and boles, also intercept varying amounts of light. They contribute to LAI derived from some detection methods and tend to the overestimation results [9]. The presence of trunks and stems is an overestimation factor to evaluate LAI based on terrestrial LiDAR measurements also [10]–[12]. Therefore, the high accuracy of LAI estimation over landscapes depends heavily on the ground-based LiDAR measurements of leaf and wood components [10]. However, it is technologically challenging to separate wood-leaf points of LiDAR data.

Many studies have explored wood-leaf separation based on certain tree measurements. There are mainly three methods based on information of objects captured by laser scanners, including intensity-based methods used radiometric information [13]–[15], geometry-based methods employed 3-D coordinates information [16]–[19], and a combination of both [20]. For lack of a good theoretical understanding of the waveform response

for different targets, distinguishing wood components from leaf components with the intensity of the reflected pulse requires significant differences in the optical properties of these components in some spectral range [10], [14], [15], [21]. Unfortunately, it is inaccurate to separate woody components from foliage based on characteristic waveform. Intensity information captured by a laser scanner needs a system-specific radiometric calibration before further utilization [22]. Normalize intensity of the return signal is employed to remove independent of the distance between the instrument and the target and screen out pulse returns from woody elements. Geometry-based methods mainly extract a set of features with its eigenvectors and normal vectors for each point [19] and classify wood and leaf at multiple spatial scales with machine learning models [16]–[19], [23]. These two methods and their combination are proposed mainly based on the terrestrial LiDAR with a single wavelength. Intensity information of the backscattered laser pulse or the spectral information is restricted by the monochromatic laser source, which influences the performance efficiency of separation [24].

Researchers proposed LiDAR equipment configurations with two laser sources of different wavelengths to improve wood and leaf separation [25]–[28]. New developed multispectral equipment might improve separation and classification accuracy. Combining several monochromatic laser sources are an instant method to obtain multispectral LiDAR beams. However, combining too many laser sources is problematic to extend the spectral band coverage and improve spectral resolution [29]–[33]. More laser sources can result in more hardware costs due to complex optic systems and volume. Another novel hyperspectral LiDAR (HSL) system employing a supercontinuum laser (SL) as an optical source has been demonstrated finer spectral resolution and wider spectral range [33], [34]. It is of great significance for spreading and promoting HSL applications in vegetation index detection and measurement by employing many laser pulses emitted from the visible to near-infrared part of the spectrum [35]–[38]. Hakala *et al.* [35] designed an HSL with 16 elements Avalanche photodiode (APD) array sensor spectral range of 470–990 nm and demonstrated the instrument’s potential in remote sensing of vegetation, constructing 3-D point clouds with backscattered reflectance and spectral indices with eight discontinuous channels. Li *et al.* [36] investigated a prototyped HSL to assess its feasibility on agriculture application and conducted the lab experiments for vegetation red edge detection based on general accuracy evaluation of range and spectral measurement. Chen *et al.* [37] designed a 10-nm spectral resolution HSL and assessed its feasibility in vegetation application. Jiang *et al.* [38] extracted the red edge position, slope, and area of plant leaves based on an HSL measurement with common extraction methods and proved it efficient and feasible for vegetation research. As we know, the red edge refers to the rapidly rising area of the green vegetation reflectance during 670–780 nm, while the reflectance of other forest components has no such characteristic [39]–[42]. The red edge area of vegetation spectral information can be explored to study the physiological and biochemical parameters [43]. Therefore, we suppose the wood–leaf separation could be conducted based on vegetation parameters in the red edge area extracted from HSL measurements.

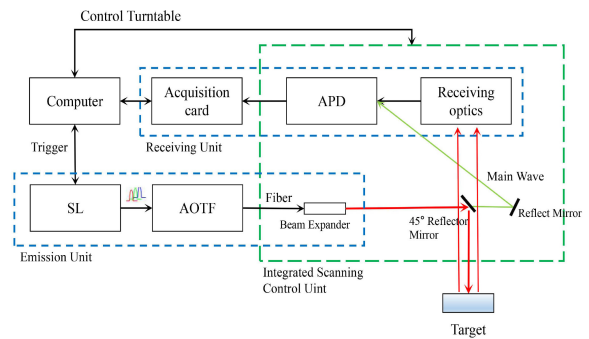


Fig. 1. Schematic setup of the revised HSL.

The HSL configuration with a continuous spectrum and a high spectral resolution was set up to obtain genuinely hyperspectral data. Excellent applications were reported in the previous literatures [37], [38]. This article will update the previous version of acousto-optic tunable filter (AOTF) based HSL by improving the scanning system. Different samples are measured to evaluate the separation feasibility of employing the spatial-spectral point cloud data from HSL in laboratory circumstances, and preprocessing is conducted based on these collected point cloud data. Furthermore, we propose a three-step wood–leaf separation method with the spectral and spatial characteristic parameters to separate leaf and wood components in 3-D reconstruction based on this revised HSL. First, we divide the selected spectrum into three segments and extract two key parameters based on hyperspectral information. Second, the wood–leaf judgment is conducted by comparing these parameters and experimental thresholds. Third, enhanced separation is conducted based on K-Nearest Neighbor (KNN) classification with the preliminary separation and spatial features. Finally, the wood–leaf separation results are fused into the 3-D spatial coordinate.

The rest of this article is organized as follows: Section II presents the revised HSL instrument and data measurements; Section III describes the proposed method. Results and analysis of the laboratory experiments are presented in Section IV. Finally, Section V concludes this article.

II. INSTRUMENT AND DATA MEASUREMENTS

A. HSL Instrument

The experimental instrument employed in this research is an HSL with high-spectral resolution to obtain hyperspectral measurements with range measurements, and more details about the instrument could be found in our recent research works [37], [38], [44]–[46]. Fig. 1 shows a schematic illustration of our revised HSL system, consisting of three parts: emission unit (EU), receiving unit (EU), and scanning system.

EU consists of a SL source, an AOTF, and a beam expander. SL delivers a broad spectral “white” laser pulse ranging from 400 to 2400 nm. The AOTF offers a quicker tuning speed and broader spectral range. We selected the spectral range from 550 to 1050 nm in the following experiments. Then, a continuous spectrum with a finer spectral resolution of 5 nm can be achieved. The laser beam expander is used to collimate the laser beam and

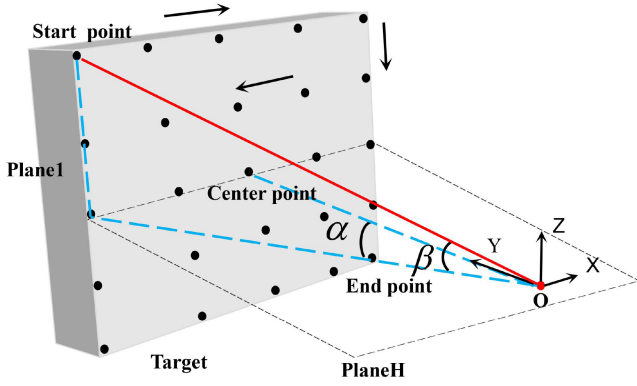


Fig. 2. HSL scanning strategy.

transfer it to the reflector mirrors. A 45° reflector mirror reflects the primary optical components of EU toward the target. The secondary reflect mirror behind the 45° reflector mirror collects a small portion of transmitting pulse as a main wave to trigger the time-of-flight (ToF) measurement.

RU consists of a receiving optics (Cassegrain telescope), APD detector, and a high-speed acquisition card with a sampling rate of 5G-points-per-second. The APD detector collects main wave signals and echo signals of the target gathered by receiving optics, transform them into electronic signals, and then amplifies them. The waveforms, including the transmitted pulse and the amplified echo, are collected by the high-speed acquisition card. The distance between the laser source and target point can be calculated by

$$D = \frac{1}{2}c\Delta t \quad (1)$$

where c represents light speed, Δt is the time interval of the main wave and echo.

The ToF measurements of different spectral channels are calculated based on the collected waveforms recorded with a simple maximum algorithm [46]–[48].

The scanning system is mainly composed of a 2-D rotating platform that can control the transmitting beam of EU and the receiving optics with stepper motor synchronously. The footprint diameter of LiDAR is about 10 mm during the lab testing. Fig. 2 shows our HSL system scanning strategy. The center point of the target (Center point) is set as a datum point. The horizontal plane (Plane H) includes the center point and laser emission point $O(x_0, y_0, z_0)$. Y-axis is the axial line that goes through O and center point, Z-axis is vertical to Plane H, and X-axis is perpendicular to Y–O–Z. The start point and the end point are confirmed, contributing to determining scan range. Scanning is performed in a zig-zag manner as following the black arrow in Fig. 2, which can reduce scanning time and decrease the rotating platform vibration. The vertical plane (Plane 1) through the start point is perpendicular to Plane H. The next vertical plane is like Plane 1. The azimuth angle α is the angle between laser beam projection in Plane H and Y-axis. The pitch angle β is the angle between laser beam projection in Plane H and the beam. If α , β , and D are available, we calculate 3-D coordinate of every

TABLE I
SAMPLE DESCRIPTION

Sampleset	Categories	Number of samples
Sampleset 1	tree leaf	6
Sampleset 2	stem bark	6
Sampleset 3	tree leaf	7
Sampleset 4	stem bark	11

scanning point by (2).

$$\begin{cases} x = x_0 + D^* \sin \alpha \\ y = y_0 + D^* \cos \alpha \\ z = z_0 + D^* \sin \beta \end{cases} \quad (2)$$

B. Sample Description

To evaluate the performance of the proposed method in the next section, we obtained spatial-spectral point cloud signals of several tree samples from leaf and bark by our HSL as tested data (Sampleset 1, Sampleset 2, Sampleset 3, and Sampleset 4). The related information is listed in Table I.

There are six species of tree samples collected from leaf (Sampleset 1) and bark (Sampleset 2), respectively: Chinese photinia (*Photinia serratifolia*), Formosan sweet gum (*Liquidambar formosana* hance), Japanese Apricot (*Armeniaca mume* Sieb.), bauhinia (*Cercis chinensis*), oriental cherry (*Prunus serrulata* var. *spontanea*), and oleander (*Nerium oleander* L.).

Sampleset three consists of seven species of tree leaf samples: clove (*Syringa oblata* Lindl.), ginkgo (*Ginkgo biloba* L.), Chinese white poplar (*Populus tomentosa* Carr), prunus davidiana (*Amygdalus davidiana* (Carrière) de Vos ex Henry), duzhong (*Eucommia ulmoides* Oliver), Yunnan Pine (*Pinus yunnanensis* faranch), and magnolia denudata (*Yulania denudata* (Desrousseaux) D. L. Fu).

There are 11 stem bark samples in Sampleset 4, including fresh wood (same species in Sampleset 2) and seasoned wood. Fresh wood bark data collected experiments were conducted within 1 h after these branches sawed off from trees. Seasoned wood samples were already dehydrated for a long time, which were provided by Key Laboratory for Silviculture and Conservation of Ministry of Education, Beijing Forestry University, including Chinese ash (*Fraxinus chinensis*), birch (*Betula platyphylla* Suk.), ailanthus (*Ailanthus altissima* (Mill.) Swingle), tortoise-shell bamboo (*Phyllostachys heterocyclus* (Carr.) Mitford cv. *Pubescens*), and goldenrain tree (*Koelreuteria paniculata* Laxm.). To ensure the validity of the collection, we measured 10 points randomly of each sample and averaged them as analysis values.

We also obtained the spatial-spectral point cloud data from magnolia denudata, crape myrtle (*Lagerstroemia indica* L.), Chinese photinia (*Photinia serrulata* Lindl.) and pachira macrocarpa (bonsai tree) that were used to simulate tree samples for their perennial trunk in the lab environment. Fig. 3 shows four different samples in the lab experiment, magnolia denudate, and pachira macrocarpa are shown in Fig. 3(c) and (d).

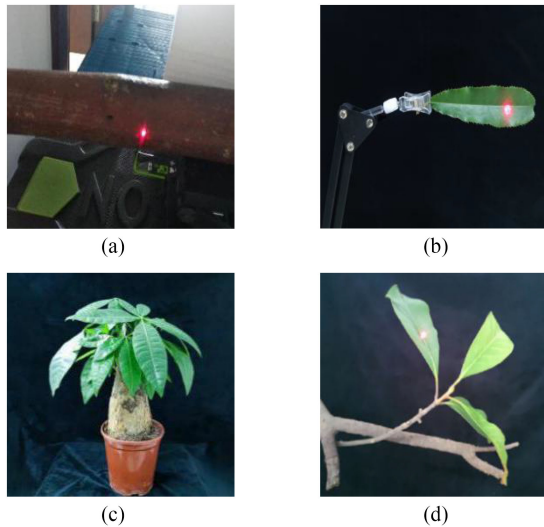


Fig. 3. Some samples (a) Goldenrain wood stem (seasoned); (b) Ginkgo leaf; (c) *Pachira macrocarpa*; (d) *Magnolia denudata* branch with leaves.

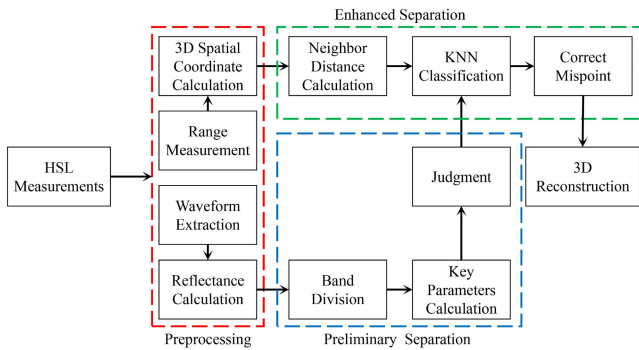


Fig. 4. Schematic diagram of the proposed method.

C. Feature Description

The data-collect experiments were conducted under a controlled lab environment to obtain hyperspectral and spatial information mainly via HSL. All samples and a standard 99% reflectivity diffuse reflection reference board were measured at a 5-m distance to collect the reliable SNR original waveforms in all spectral channels. The echo intensities which can record the target reflected powers were collected and quantized by the quantizer with 8-b depth equaling to an interval of 3.9 milli-volts. The reflectance is the calibrated echo intensity. As a prerequisite for many quantitative applications, it has recently become an important research topic [38], [44]–[47]. In this research, LiDAR calibration conducted assisted with the reference board during the experiments, as reference [33], [37], [38].

III. METHOD

Fig. 4 shows the proposed wood–leaf separation method’s schematic diagram, which includes four parts: preprocessing, preliminary separation based on spectral features, enhanced separation based on spatial geometry features, and 3-D reconstruction.

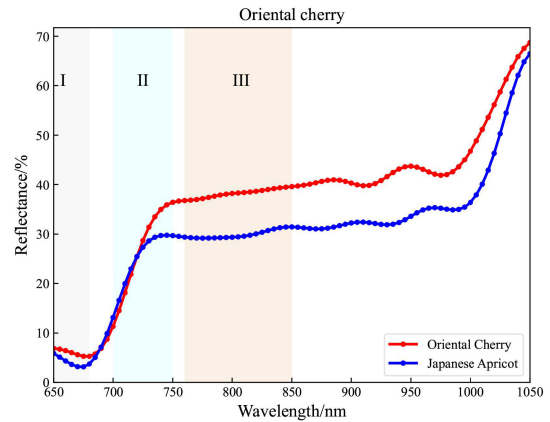


Fig. 5. Three reflectance segments of two tree leaf samples (I, II, and III denotes Segment 1, 2, and 3, respectively).

The preprocessing part includes range measurements, 3-D spatial coordinate calculation and reflectance calculation and waveform extraction, which has been discussed in Section II. Preliminary separation consists of band division and wood–leaf separation with reflectance (key parameters calculation and judgment). After that, enhanced separation is conducted by KNN based on previous judgment and then update the results by re-correction. Moreover, the results are visualized straightforwardly with 3-D reconstruction.

A. Preliminary Separation

1) *Band Division*: The corresponding vegetation parameters are widely estimated, relying on chlorophyll absorption, creating low reflectance in the red spectral range and high reflectance in the near-infrared (NIR) spectral range due to the scattering of light from the intercellular volume of leaf mesophyll [13], [49].

For the deep concentration of chlorophyll shown by spectrum starting from 680 to 800 nm of leaves [50], red and red edge position can help us to acquire the vegetation situation. In this research, we investigate leaf features based on three segments: red band (650–680 nm), red-edge (700–750 nm), NIR (760–850 nm), as reference [49] defined. The band division is based on HSL reflectance, as Fig. 5 shown. Segment 1 has low reflectance due to chlorophyll absorption in this red spectral region [51]. Segment 2 has a sharp reflectance change called red-edge region position, which shifts to longer wavelengths based on an increase in leaf chlorophyll content [43], [49], [52]. The variation in chlorophyll content and LAI contributes to obtaining the leaf information based on spectral reflectance. Segment 3 has high reflectance for the cellular scattering of leaf mesophyll in the NIR spectral region [49], [53], and the reflectance distribution is flat in this range. Therefore, we select 31-channel reflectance in the spectral range from 650 to 850 nm. And the tests will be conducted within this range in the following sections.

Fig. 6 shows the reflectance of collecting data from the bark and the leaf of Formosan sweet gum and oriental cherry tree in test range (650 nm, 850 nm), called wood and leaf component. The reflectance tendencies of the two samples are similar. However, as we can see, the wood reflectance is flatter than the

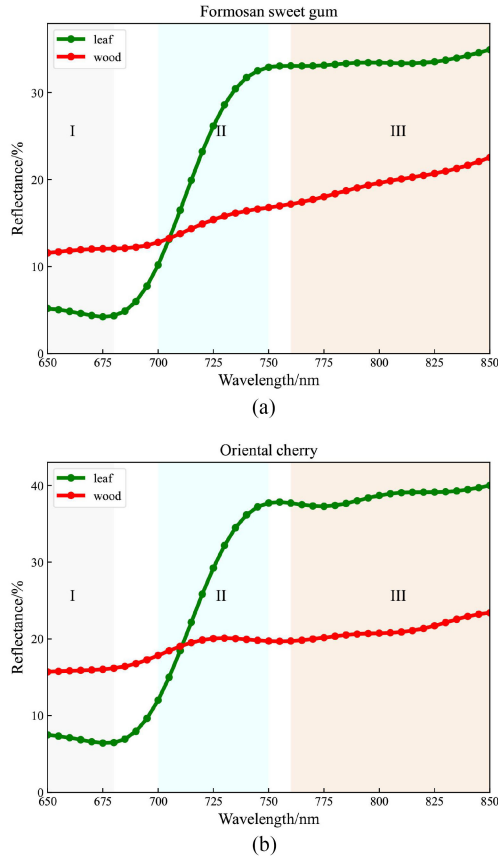


Fig. 6. Reflectance distribution of wood and leaf samples (a) Formosan sweet gum; (b) Oriental cherry.

leaf reflectance in Segment 1. The reflectance variation tendencies of wood and leaf component are considerably different in Segment 2, and their reflectance curves are even in Segment 3.

2) *Wood–Leaf Separation With Reflectance*: First of all, we discuss two key parameter descriptors of spectral segments. As we know, the foliage reflectance value in Segment 1 is low and stable, and Segment 3 has high and unfluctuating reflectance values. Therefore, we calculate the ratio of Segment 3 and Segment 1 (namely Ratio) by (3) to explore the difference between the leaf component and others.

$$\text{Ratio} = \frac{\frac{1}{M} \sum_{760+i}^{760+M} R_i}{\frac{1}{N} \sum_{650+j}^{650+N} R_j} \quad (3)$$

where R represents reflectance. M is the channel number of Segment 3, and N is the channel number of Segment 1. We will select the ratio of Segment 3 and Segment 1 as the parameter value for the first step estimate. Then, we compare Ratio with an experiment threshold $T1$ to estimate the tested sample in this range belongs to the tree leaf class or other sample classes probably.

We observe that there is a sharp fluctuation in Segment 2, so the first derivative (FD) of spectral reflectance R' can be expressed as the following equation to obtain reliable feature

TABLE II
PARAMETER CALCULATED VALUES OF LEAF SAMPLES

Sampleset 1	1	2	3	4	5	6
Ratio	4.01	7.18	7.82	10.23	5.59	6.29
FD	0.58	0.45	0.30	0.51	0.51	0.50

parameters for foliage and wood components in segment 2:

$$R_1' = \frac{R_{750} - R_{700}}{\lambda_{750} - \lambda_{700}} \quad (4)$$

We select two key points at 750 and 700 nm in the red-edge range to calculate FD value, where R, λ represent reflectance and wavelength, respectively. R_1' is the second decision parameter employed to compare with a threshold $T2$ for further judgment.

The judgment processing is conducted by comparing feature parameters with these thresholds ($T1, T2$), which will be determined by experiments in the next section. While ratio is greater than $T1$ and R' is greater than $T2$ simultaneously, the sample is judged as a tree leaf component. Likewise, while Ratio is less than $T1$ and R' is less than $T2$ simultaneously, the sample is judged as a tree bark component. Otherwise, we define the sample as an uncertain component.

B. Enhanced Separation

There are two uncertain component situations: Ratio is greater than $T1$ and R' is less than $T2$; Ratio is less than $T1$ and R' is greater than $T2$. To classify uncertain components exactly, we introduce enhanced separation based on KNN classification with spatial coordinate information. Suppose that point $A(x, y, z)$ is an uncertain component point to be judged, point $B_j(x_j, y_j, z_j)$ is a certain component point. We calculate the distance $dist_i$ between A and B_j . n points around A in a given distance (1 mm) are searched. The first K minimal values are selected from these n sorted points, and K is set 7 according to our experiences. The enhanced separation is conducted based on preliminary separation results. Point A will be classified into leaf component if the number of leaf points is greater than the wood points. Otherwise, it would be classified into a wood component.

If there are wrong separation points inevitably, we recorrected these points based on the actual reflectance feature.

IV. RESULTS AND ANALYSIS

A. Threshold Determination

We tested Sampleset 1 and Sampleset 2 to confirm the experimental thresholds. Table II lists the parameter values of leaf samples in Sampleset 1. The minimum ratio value of leaf samples is 4.01, and the maximum value is 10.23. The minimum FD value in the second row is 0.30, and the maximum value is 0.58.

Table III lists the key parameter results of wood samples in Sampleset 2. The minimum ratio value is 1.33, and the maximum value is 1.96. The minimum FD value is 0.04, and the maximum value is 0.12.

TABLE III
PARAMETER CALCULATED VALUES OF WOOD SAMPLES

Sampleset 2	1	2	3	4	5	6
Ratio	1.96	1.66	1.59	1.77	1.33	1.62
FD	0.10	0.08	0.07	0.12	0.04	0.08

TABLE IV
PARAMETER CALCULATED VALUES OF SAMPLESET 3 SAMPLES

Sampleset 3	1	2	3	4	5	6	7
Ratio	13.78	9.84	14.83	18.54	8.74	17.62	7.00
FD	0.76	0.73	0.72	0.61	0.73	0.74	0.66

TABLE V
PARAMETER CALCULATED VALUES OF SAMPLESET 4 SAMPLES

Sampleset 4	1	2	3	4	5	6
Ratio	1.80	1.61	1.52	1.93	1.47	1.19
FD	0.12	0.06	0.05	0.15	0.07	0.03

Sampleset 4	7	8	9	10	11
Ratio	1.41	1.24	1.11	1.33	1.96
FD	0.02	0.05	0.04	0.02	0.04

Considering enlarging the threshold tolerance, we initially set the threshold T1 and T2 as 2 and 0.2, respectively, based on Tables I and II. However, we could not confirm these decided thresholds, and we will further test whether these thresholds of the proposed method are practicable.

B. Preliminary Separation Performance

To honestly evaluate the proposed method performance for wood–leaf separation, the hyperspectral features extracted from Sampleset 3 and Sampleset 4 are tested. Table IV shows the results of calculated values. Every ratio is far greater than T1 (2). Meanwhile, every value of FD is greater than T2 (0.2). Therefore, the parameter values all satisfy the double thresholding judgment of the proposed method in the previous section. Based on the thresholding judgment, the conclusion can be drawn, samples in Sampleset 3 belong to tree foliage.

As Table V listed, each ratio is less than 2, and FD is far less than 0.2, which also satisfies the double thresholding judgment. Therefore, we estimate that these eleven samples belong to wood component.

Fig. 7 shows the preliminary separation result of the bonsai tree sample in Fig. 3(c). Fig. 7(a) shows the scanning points of this sample. The proposed preliminary separation method can successfully separate most leaf points and wood points [see Fig. 7(b)], representing different components with different colors (green: leaf, yellow: wood, red: uncertain component). There are some misclassification points in the leaf parts, obviously, especially on the edge of the leaves. Fig. 7(c) shows the improved display result by the point expansion method to meet visual requirements.

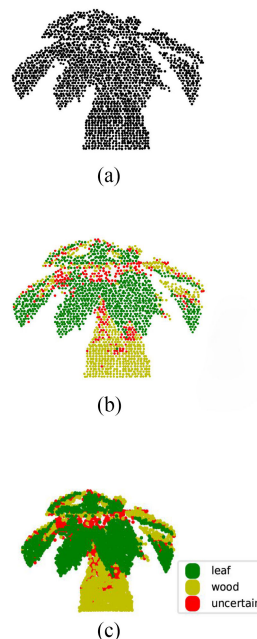


Fig. 7. Performance of preliminary separation (a) The scanning point image; (b) Preliminary separation result; (c) Preliminary separation visualization.

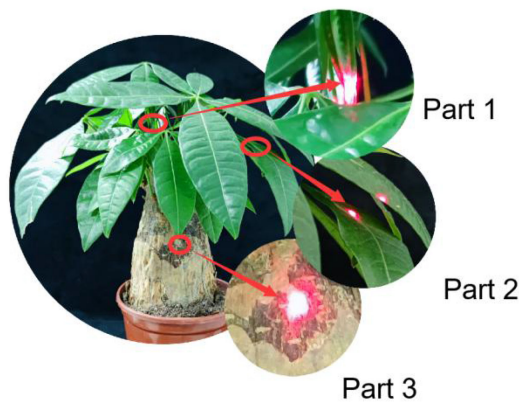


Fig. 8. Three picked misclassification parts in Fig. 7(b).

We also observed some uncertain points in Fig. 7(b). One situation is that the green shoots (Part 1 in Fig. 8) are misjudged. Another situation is that its stem bark (Part 3) was broken by accident. The tissue under the bark is green, which is judged as a leaf component. The reason for most misclassified points is that the angle between the HSL incident laser beam and leaf target incident angle is larger than 90° , and the footprint does not focus on one point, which is dispersed on two different leaves, and some portion of the laser beam dissipate into the air, as Part 2, namely Edge Point.

We further analyze three parts' reflectance with two normal points (true leaf point, true wood point), which are presented in Fig. 9. Table VI lists the key parameters of these five points. The reflectance slope of Part 1 is much gentler than the true leaf point, in which the FD value (0.17) is smaller than T2. Nevertheless, their reflectance values in Segment 1 are close, and their reflectance values in Segment 3 are stable. The mean

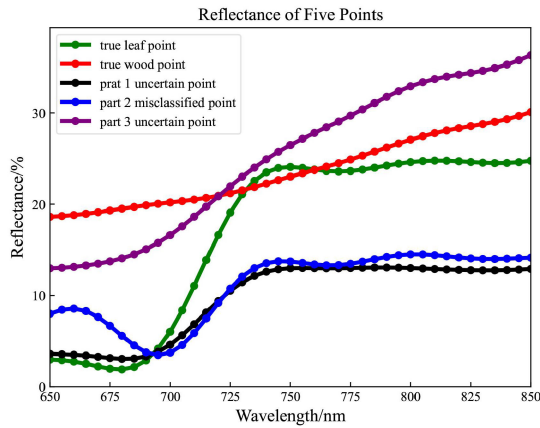


Fig. 9. Comparison of different parts.

 TABLE VI
 KEY PARAMETERS OF DIFFERENT POINTS

Sample Point	leaf	wood	Part1	Part2	Part3
Ratio	9.80	1.43	3.82	1.84	2.44
FD	0.36	0.06	0.17	0.19	0.19

reflectance value of Part 1 is 47% less than that of true leaf points in Segment 3. But its Ratio value (3.82) is bigger than T1.

As for Part 3 point compared with the true wood point, we can see the reflectance uptrend of the true wood point is weaker than that of Part 3 point, mean reflectance value of Part 3 point is 4% larger than that of true wood point in the tested spectrum. The ratio value (2.44) of Part 3 is bigger than T1, and its FD value (0.19) is smaller than T2. According to our primary method, both of the two parts belong to the uncertain components.

Part 2 point (Edge Point) reflectance slope of Segment 2 is gentler than true leaf point, and FD value (0.19) is smaller than T2. But there is a sharp variation in Segment 1 comparing with the true leaf point and a stable variation in Segment 3. The mean reflectance value of Part 2 is 67% larger than the true leaf point in Segment 1 and 42% smaller than that in Segment 3. So its ratio value (1.84) is smaller than T1, which was misclassified into wood point according to our primary method.

As shown in Fig. 9, the reflectance of Part 2 point at leaf edge has a sharp descending tendency from 670 to 700 nm. We selected 20 misclassified points at the edge location randomly and further analyzed reflectance distribution (see Fig. 10). It can be seen that their reflectance has similar characteristics. There is a rising trend from 650 to 670 nm, a sharp descending tendency from 670 to 700 nm, and an escalating range (700 nm, 850 nm). It has a great difference between normal leaf point and edge point. So, we can further separate them by (5).

$$R'_2 = \frac{R_{670} - R_{700}}{\lambda_{670} - \lambda_{700}} \quad (5)$$

where R'_2 represents the FD spectrum from 670 to 700 nm, R , λ represent reflectance and wavelength, respectively. While its absolute value is bigger than 0.05, we set this misjudged point as an edge point.

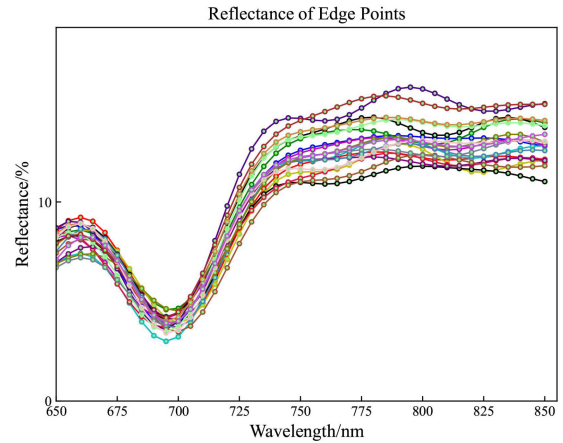


Fig. 10. Reflectance of Edge Points.

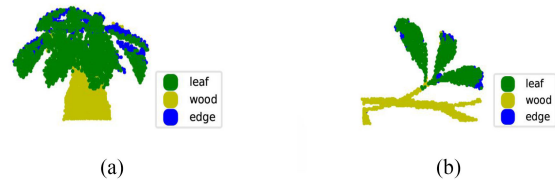


Fig. 11. Enhanced separation with KNN.

C. Enhanced Separation Performance

Fig. 11(a) shows the modified results of Fig. 7(c) based on the enhanced separation. Fig. 11(b) is the separation results of the branches in Fig. 3(d). As can be seen, our method can separate the leaf and wood components very well. However, there are some misclassification points at leaf parts. The reasons for the wrong separation probably are as follows: one reason is that the footprint of our HSL is not small enough to obtain the detail of the tree, which captures one portion of the HSL beam on the edge of the target, and another portion of the HSL beam is disappeared in the air (or absorbed by the background), and the echo signal is weakened. Therefore, the calculated reflectance does not satisfy the leaf feature. Another reason is that the free-growing leaves have their tilt angles, and the angles between the laser beam and these leaves are different, and even some angles are obtuse.

D. Separation Accuracy

To assess the performance of our method, we projected the HSL point cloud to a 2-D image collected by a mobile phone (MI 10, 100 megapixels), as presented in Fig. 12. For a diverse view of these two acquisition devices, there are some mismatched points. However, with every point registration from the same position of the image, if the leaf point judged by our method is locating at the leaf area in the image, we define this point as the correct leaf point. Similarly, we can define the correct wood point. The separation accuracy of the leaf component is the ratio of correct leaf points to total leaf points. The separation accuracy of the wood component is calculated in the same way.



Fig. 12. Registration of HSL point cloud and 2D image.

TABLE VII
SEPARATION ACCURACY

Samples	leaf	wood	total
Pachira macrocarpa	82.75%	97.33%	86.08%
Magnolia denudata	89.91%	96.59%	92.34%
Crape myrtle	91%	96.43%	91.7%
Chinese photinia	94.69%	97.38%	95.69%

Table VII lists the separation accuracy, which indicates our method can obtain very good classification results. The separation accuracy of wood components is higher than the leaf components. The leaf separation of magnolia denudate branches exceeds pachira macrocarpa's 7.16%, 8.25%, and 11.94%, respectively. The leaves on the magnolia branch and Chinese photinia branch are rare, and their tilt angles are not bigger enough to generate less edge points, so separation results are ideal. The crape myrtle branch leaves are much dense than the other branches, but its tilt angles are also not obvious so that the separation result is perfect. The leaves on pachira macrocarpa are dense, and the distribution of incident angle is more fluctuating. Therefore, its leaf separation is not ideal. All the samples show similar wood separation results, which indicate the proposed method is promising for wood extraction. Combining with leaf accuracy, the total accuracy of branches exceeds 6.26%, 5.62%, 9.61% than that of pachira macrocarpa, respectively.

V. CONCLUSION

Our investigation was conducted to separate wood and leaf components with a proposed method based on HSL measurements. We demonstrated that our proposed method could judge wood and leaf points simply and directly to obtain the desired separation results for forest applications. First, we updated the revised HSL by improving the scanning strategy. Then, the preprocessing was conducted based on HSL measurements in laboratory circumstances. The preliminary separation with reflectance, including band division, key parameter calculation, and judgment. And then enhanced separation based on KNN further improved the separation performance. However, the desired result was not attained. It was just the beginning using the

high spectral resolution HSL for leaf and wood detection, which might simplify the forest 3-D construction.

This work discussed the potential forest applications of wood-leaf separation with HSL measurements. Our future work is to design leaf and wood detection models that satisfy different trees in a forest and improve the 3-D reconstruction effect. Furthermore, we will discuss the relation and difference of spatial-spectral features of different species trees in forest surveys. We also plan to develop an advanced compacted HSL for recording and quantifying the structural complexity of forests.

ACKNOWLEDGMENT

The authors acknowledge the support of Key Laboratory for Silviculture and Conservation of Ministry of Education, Beijing Forestry University for the seasoned wood samples.

REFERENCES

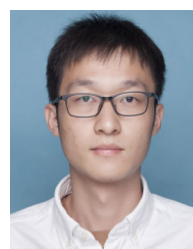
- [1] A. Wehr and U. Lohr, "Airborne laser scanning—an introduction and overview," *ISPRS J. Photogramm. Remote Sens.*, vol. 54, pp. 68–82, 1999.
- [2] L. P. Bentley *et al.*, "An empirical assessment of tree branching networks and implications for plant allometric scaling models," *Ecol. Lett.*, vol. 16, pp. 1069–1078, Jun. 2013.
- [3] S. L. Tao, Q. H. Guo, S. W. Xu, Y. J. Su, Y. M. Li, and F. F. Wu, "A geometric method for wood-leaf separation using terrestrial and simulated Lidar data," *Photogrammetric Eng. Remote Sens.*, vol. 81, no. 10, pp. 767–776, Oct. 2015.
- [4] M. J. Ducey, R. Astrup, S. Seifert, H. Pretzsch, B. C. Larson, and K. D. Coates, "Comparison of forest attributes derived from two terrestrial Lidar systems," *Photogrammetric Eng. Remote Sens.*, vol. 79, no. 3, pp. 245–257, Mar. 2013.
- [5] T. Yao *et al.*, "Measuring forest structure and biomass in new england forest stands using Echidna ground-based Lidar," *Remote Sens. Environ.*, vol. 115, no. 11, pp. 2965–2974, Nov. 2011.
- [6] F. Zhao *et al.*, "Measuring effective leaf area index, foliage profile, and stand height in New England forest stands using a full-waveform ground-based lidar," *Remote Sens. Environ.*, vol. 115, no. 11, pp. 2954–2964, Feb. 2011.
- [7] L. R. Jensen, K. S. Humes, L. A. Vierling, and A. T. Hudak, "Discrete return Lidar based prediction of leaf area index in two conifer forests," *Remote Sens. Environ.*, vol. 112, no. 10, pp. 3947–3957, Oct. 2008.
- [8] D. B. Clark, P. C. Olivas, S. F. Oberbauer, D. A. Clark, and M. G. Ryan, "First direct landscape-scale measurement of tropical rain forest leaf area index, a key driver of global primary productivity," *Ecol. Lett.*, vol. 11, pp. 163–172, 2008.
- [9] Z. Li *et al.*, "Separating leaves from trunks and branches with dual-wavelength terrestrial lidar scanning," in *Proc. IEEE Int. Geosci. Remote Sens. Symp.* Melbourne, VIC, Australia, Jul. 2013, pp. 3383–3386.
- [10] D. L. B. Jupp, D. S. Culvenor, J. L. Lovell, G. J. Newnham, A. H. Strahler, and C. E. Woodcock, "Estimating forest LAI profiles and structural parameters using a ground-based laser called Echidna(R)," *Tree Physiol.*, vol. 29, no. 2, pp. 171–181, Feb. 2008.
- [11] T. Nilson and A. Kuusk, "Improved algorithm for estimating canopy indices from gap fraction data in forest canopies," *Agricultural Forest Meteorol.*, vol. 124, pp. 157–169, Aug. 2004.
- [12] X. Zhu *et al.*, "Improving leaf area index (LAI) estimation by correcting for clumping and woody effects using terrestrial laser scanning," *Agricultural Forest Meteorol.*, vol. 263, pp. 276–286, Dec. 2018.
- [13] J. F. Cote, J. L. Widlowski, R. A. Fournier, and M. Verstraete, "The structural and radiative consistency of three-dimensional tree reconstructions from terrestrial lidar," *Remote Sens. Environ.*, vol. 113, no. 5, pp. 1067–1081, May 2009.
- [14] G. Fitzgerald, D. Rodriguez, and G. O'Leary, "Measuring and predicting canopy nitrogen nutrition in wheat using a spectral index - The canopy chlorophyll content index (CCCI)," *Field Crop. Res.*, vol. 116, no. 3, pp. 318–324, Apr. 2010.
- [15] M. Béland, D. D. Baldocchi, J. L. Widlowski, R. A. Fournier, and M. M. Verstraete, "On seeing the wood from the leaves and the role of voxel size in determining leaf area distribution of forests with terrestrial LiDAR," *Agricultural Forest Meteorol.*, vol. 184, pp. 82–97, Jan. 2014.

- [16] L. Ma, G. Zheng, J. U. H. Eitel, L. M. Moskal, W. He, and H. Huang, "Improved salient feature-based approach for automatically separating photosynthetic and non-photosynthetic components within terrestrial LiDAR point cloud data of forest canopies," *IEEE Trans. Geosci. Remote Sens.*, vol. 54, no. 2, pp. 679–696, Feb. 2016.
- [17] M. B. Vicari, M. Disney, P. Wilkes, A. Burt, K. Calders, and W. Woodgate, "Leaf and wood classification framework for terrestrial LiDAR point clouds," *Methods Ecol. Evol.*, vol. 10, pp. 680–694, Jan. 2019.
- [18] X. Y. Yang *et al.*, "Three dimensional forest reconstruction and structural parameter retrievals using a terrestrial full-waveform Lidar instrument (Echidna (R)),", *Remote Sens. Environ.*, vol. 135, pp. 36–51, Aug. 2013.
- [19] S. Moorthy, M. Calders, M. Boni Vicari, and H. Verbeeck, "Improved supervised learning-based approach for leaf and wood classification from LiDAR point clouds of forests," *IEEE Trans. Geosci. Remote Sens.*, vol. 58, no. 5, pp. 3057–3070, May 2020.
- [20] K. Koenig, B. Höfle, M. Hämmerle, T. Jarmer, B. Siegmann, and H. Lilienthal, "Comparative classification analysis of post-harvest growth detection from terrestrial LiDAR point clouds in precision agriculture," *ISPRS J. Photogramm. Remote Sens.*, vol. 104, pp. 112–125, Jun. 2015.
- [21] V. Ducic, M. Hollaus, A. Ullrich, W. Wagner, and T. Melzer, "3D Vegetation mapping and classification using fullwaveform laser scanning," in *Proc. Workshop 3D Remote Sens. Forestry*, Vienna, Austria, Feb. 2006, pp. 211–217.
- [22] K. Calders *et al.*, "Evaluation of the range accuracy and the radiometric calibration of multiple terrestrial laser scanning instruments for data interoperability," *IEEE Trans. Geosci. Remote Sens.*, vol. 55, no. 5, pp. 2716–2724, May 2017.
- [23] T. Yun, F. An, W. Li, Y. Sun, L. Cao, and L. Xue, "A novel approach for retrieving tree leaf area from ground-based LiDAR," *Remote Sens.*, vol. 8, pp. 942, 2016.
- [24] S. Kaasalainen, T. Lindroos, and J. Hyypä, "Toward hyperspectral lidar: Measurement of spectral backscatter intensity with a supercontinuum laser source," *IEEE Geosci. Remote Sens. Lett.*, vol. 4, no. 2, pp. 211–215, Apr. 2007.
- [25] S. Hancock, R. Gaulton, and F. M. Danson, "Angular reflectance of leaves with a dual-wavelength terrestrial lidar and its implications for leaf-bark separation and leaf moisture estimation," *IEEE Trans. Geosci. Remote Sens.*, vol. 55, no. 6, pp. 3084–3090, Jun. 2017.
- [26] E. S. Douglas *et al.*, "Finding leaves in the forest: The dual-wavelength Echidna lidar," *IEEE Geosci. Remote Sens. Lett.*, vol. 12, no. 4, pp. 776–780, Apr. 2015.
- [27] F. M. Danson, F. Sasse, and L. A. Schofield, "Spectral and spatial information from a novel dual-wavelength full-waveform terrestrial laser scanner for forest ecology," *Interface Focus*, vol. 8, Feb. 2018, Art. no. 20170049.
- [28] Z. Li, A. Strahler, C. Schaaf, D. Jupp, M. Schaefter, and P. Olofsson, "Seasonal change of leaf and woody area profiles in a midlatitude deciduous forest canopy from classified dual-wavelength terrestrial lidar point clouds," *Agricultural Forest Meteorol.*, vol. 262, pp. 279–297, Nov. 2018.
- [29] J. U. Eitel *et al.*, "Beyond 3-D: The new spectrum of lidar applications for earth and ecological sciences," *Remote Sens. Environ.*, vol. 186, pp. 372–392, Dec. 2016.
- [30] W. Li, G. Sun, Z. Niu, S. Gao, and H. Qiao, "Estimation of leaf biochemical content using a novel hyperspectral full-waveform LiDAR system," *Remote Sens. Lett.*, vol. 5, no. 8, pp. 693–702, Sep. 2014.
- [31] L. Du *et al.*, "Estimation of rice leaf nitrogen contents based on hyperspectral LiDAR," *Int. J. Appl. Earth Obs.*, vol. 44, pp. 136–143, Feb. 2016.
- [32] J. Sun *et al.*, "Evaluation of hyperspectral LiDAR for monitoring rice leaf nitrogen by comparison with multispectral LiDAR and passive spectrometer," *Sci. Rep.-U.K.*, vol. 7, 2017, Art. no. 40362.
- [33] Y. W. Chen, "Environmental awareness with hyperspectral LiDAR," Ph.D. dissertation, Dept. Comp. Sci., Aalto Univ., Helsinki, Finland, 2020.
- [34] J. Suomalainen, T. Hakala, H. Kaartinen, E. Räikkönen, and S. Kaasalainen, "Demonstration of a virtual active hyperspectral LiDAR in automated point cloud classification," *ISPRS J. Photogramm.*, vol. 66, no. 5, pp. 637–641, Sep. 2011.
- [35] T. Hakala, J. Suomalainen, S. Kaasalainen, and Y. W. Chen, "Full waveform hyperspectral LiDAR for terrestrial laser scanning," *Opt. Exp.*, vol. 20, no. 7, pp. 7119–7127, 2012.
- [36] W. Li, C. H. Jiang, Y. W. Chen, J. Hyypä, L. L. Tang, and S. W. Wang, "A liquid crystal tunable filter-based hyperspectral LiDAR system and its application on vegetation red edge detection," *IEEE Geosci. Remote Sens. Lett.*, vol. 16, no. 2, pp. 291–295, Feb. 2019.
- [37] Y. W. Chen *et al.*, "A 10-nm spectral resolution hyperspectral LiDAR system based on an acousto-optic tunable filter," *Sensors*, vol. 19, no. 7, 2019, Art. no. 1620.
- [38] C. H. Jiang *et al.*, "Study of a high spectral resolution hyperspectral LiDAR in vegetation red edge parameters extraction," *Remote Sens.*, vol. 11, no. 17, Aug. 2019, Art. no. 2007.
- [39] R. L. Pu, P. Gong, G. S. Biging, and M. R. Larrieu, "Extraction of red edge optical parameters from hyperion data for estimation of forest leaf area index," *IEEE Trans. Geosci. Remote.*, vol. 41, no. 4, pp. 916–921, Apr. 2003.
- [40] F. Q. Yao, Z. H. Zhang, R. Y. Yang, J. W. Sun, and S. F. Cui, "Hyperspectral models for estimating vegetation chlorophyll content based on red edge parameter," *Trans. CSAE*, vol. 25, pp. 123–129, 2009.
- [41] P. J. Zarco-Tajeda, J. R. Miller, D. Haboudane, N. Tremblay, and S. Apostol, "Detection of chlorophyll fluorescence in vegetation from airborne hyperspectral CASI imagery in the red edge spectral region," in *Proc. IEEE Int. Geosci. Remote Sens. Symp.*, Anchorage, AK, USA, 2003, pp. 598–600.
- [42] C. Y. Pu, H. Huang, and P. L. Yang, "An attention-driven convolutional neural network-based multi-level spectral-spatial feature learning for hyperspectral image classification," *Expert Syst. Appl.*, vol. 185, no. 15, Jul. 2021, Art. no. 115663.
- [43] D. N. H. Horler, M. Dockray, and J. Barber, "The red edge of plant leaf reflectance," *Int. J. Remote Sens.*, vol. 4, no. 2, pp. 273–288, 1983.
- [44] H. Shao *et al.*, "Feasibility study on hyperspectral LiDAR for ancient huizhou-style architecture preservation," *Remote Sens.*, vol. 12, 2020, Art. no. 88.
- [45] H. Shao *et al.*, "A 91-Channel hyperspectral LiDAR for coal/rock classification," *IEEE Geosci. Remote Sens. Lett.*, vol. 17, no. 6, pp. 1052–1056, Jun. 2020.
- [46] Y. W. Chen *et al.*, "Feasibility study of ore classification using active hyperspectral LiDAR," *IEEE Geosci. Remote Sens. Lett.*, vol. 15, no. 11, pp. 1785–1789, Nov. 2018.
- [47] H. Shao *et al.*, "An investigation of spectral band selection for hyperspectral LiDAR technique," *Electronics*, vol. 9, 2019, Art. no. 148.
- [48] Z. Wang *et al.*, "Hyperspectral LiDAR with eight channels covering from VIS to SWIR," in *Proc. IEEE Int. Geosci. Remote Sens. Symp.*, Valencia, Spain, Jul. 2018, pp. 4293–4296.
- [49] Q. Y. Xie *et al.*, "Vegetation indices combining the red and red-edge spectral information for leaf area index retrieval," *IEEE J. Sel. Topics Appl. Earth Observ. Remote Sens.*, vol. 11, no. 5, pp. 1482–1493, May 2018.
- [50] P. K. Das, K. K. Choudhary, B. Laxman, S. V. C. Kameswara Rao, and M. V. R. Seshasai, "A modified linear extrapolation approach towards red edge position detection and stress monitoring of wheat crop using hyperspectral data," *Int. J. Remote Sens.*, vol. 35, pp. 1432–1449, 2014.
- [51] J. Rouse, J. R. Haas, J. Schell, and D. Deering, "Monitoring vegetation systems in the great plains with ERTS," *NASA*, vol. 351, pp. 309–317, 1974.
- [52] J. G. P. W. Clevers *et al.*, "Derivation of the red edge index using the MERIS standard band setting," *Int. J. Remote Sens.*, vol. 23, no. 16, pp. 3169–3184, Nov. 2002.
- [53] J. Delegado, J. Verrelst, C. Meza, J. Rivera, L. Alonso, and J. Moreno, "A red-edge spectral index for remote sensing estimation of green LAI over agroecosystem," *Eur. J. Agronomy.*, vol. 46, pp. 42–52, 2013.



Hui Shao received the Ph.D. degree in optics from the University of Chinese Academy of Sciences, Hefei, China, in 2014.

She is currently an Associate Professor with the School of Electronic and Information Engineering, Anhui Jianzhu University, and a Visiting Scholar with Finnish Geospatial Research Institute Finland. Her main research activities are in the fields of LiDAR, image processing, and hyperspectral remote sensing.



Zheng Cao received the B.E. degree in network engineering from West Anhui University, Luan, China, in 2018. He is currently working toward the master's degree in computer technology with Anhui Jianzhu University, Hefei, China.

His research interests are hyperspectral LiDAR, LiDAR data processing, and 3-D modeling.



Wei Li received the Ph.D. degree in engineering from the University of Chinese Academy of Sciences, Beijing, China, in 2018.

He is currently an Associate Professor with the Institute of Unmanned System, Beihang University, Beijing, China. His main research activities are in the fields of hyperspectral LiDAR, hyperspectral camera, mini UAV-borne LiDAR, and the integration of air-borne remote sensing systems.



Yuwei Chen received the B.E. degree in electronics engineering and the M.Sc. degree in circuits and systems from the Department of Information Science and Electronics Engineering, Zhejiang University, Hangzhou, China, in 1999 and 2002, respectively, and the Ph.D. degree in physical electronics and communication software from the Shanghai Institute of Technical Physics, Chinese Academy of Sciences, Shanghai, China, in 2005.

He is working with the Finnish Geospatial Research Institute, Kirkkonummi, Finland, as the Research Manager, where he leads the research group "Remote Sensing Electronics," which focuses on developing new remote sensing systems. He is also a Guest Professor with the Academy of Opto-Electronics, Chinese Academy of Sciences, Beijing, China. He holds 13 patents and has authored and coauthored more than 200 scientific articles and book chapters. His research interests include LiDAR, hyperspectral LiDAR, radar, and navigation and positioning.



Changhui Jiang received the B.S. degree in electrical engineering and automation from Soochow University, Jiangsu, China, in 2014, and the Ph.D. degree in control science and engineering from Nanjing University of Science and Technology, Nanjing, China, in 2019.

He studied as a visiting Ph.D. student with the Finnish Geospatial Research Institute (FGI) from December 2017 to November 2018 (sponsored by the China Scholarship Council (CSC)). Currently, he is working as a Research Scientist with the Finnish Geospatial Research Institute. He has authored or coauthored more than 50 published journal and conference papers. His research interests include hyperspectral LiDAR, GNSS signal processing and multisensor integration.



Juha Hyypä received the M.Sc. degree in radio engineering, the Dr.Eng. degree in space technology, and the Dr.Sc. degree (hons.) in electrical engineering from the Helsinki University of Technology, Espoo, Finland, in 1987, 1990, and 1994, respectively.

He is currently a Professor of remote sensing and photogrammetry and the Director of the Center of Excellence in Laser Scanning Research, Finnish Geospatial Research Institute, Kirkkonummi, Finland, and also a Distinguished Professor with Shinshu University, Matsumoto, Japan. He has 30 years of experience in research team leadership and in the coordination of over ten international science projects. He has authored more than 300 ISI Web of Science listed papers with more than 20000 Google Scholar citations. His research interests include laser scanning systems, their performance and new applications, especially related to mobile, personal, and ubiquitous laser scanning, and their point cloud processing especially to forest information extraction.



Jie Chen received the M.S. degree in control theory and control engineering from the University of Science and Technology of China, Hefei, China, in 2001.

He is currently a Professor with the School of Electronic and Information Engineering, Anhui Jianzhu University. His main research activities are in the fields of image processing, and control engineering.



Long Sun received the Ph.D. degree in guidance navigation and control from Harbin Engineering University, Harbin, China, in 2015.

He is currently a Senior Engineer with the School of Electronic and Information Engineering, Anhui Jianzhu University, Hefei, China. His main research activities are in the fields of millimeter-wave radar and terahertz imaging technology.